Preparation and orientation of solid ^{3}He crystals for neutron diffraction investigations

2008 J. Phys.: Condens. Matter 20 104246

(http://iopscience.iop.org/0953-8984/20/10/104246)

IOP PUBLISHING JOURNAL OF PHYSICS: CONDENSED MATTER

J. Phys.: Condens. Matter **20** (2008) 104246 (6pp) doi:10.1088/0953-8984/20/10/104246

Preparation and orientation of solid ^{3}He crystals for neutron diffraction investigations

V Boiko[1], S Matas[1,2] and K Siemensmeyer[1]

[1] Hahn Meitner Institut, Glienicker Straße 100, D-14109 Berlin, Germany
[2] Institute of Experimental Physics, Slovak Academy of Science, Watsonova 47, SK-04301 Kosice, Slovakia

E-mail: siemensmeyer@hmi.de

Received 17 July 2007, in final form 5 September 2007
Published 19 February 2008
Online at stacks.iop.org/JPhysCM/20/104246

Abstract

We have prepared solid ^{3}He crystals under constant volume conditions and characterized them by neutron diffraction and transmission. The ultimate aim of the work was the preparation of samples suitable for neutron diffraction investigations of the antiferromagnetic nuclear ordering of solid ^{3}He below 1 mK. We describe results from different sample cells, and we have derived the relevant design parameters with respect to (a) the neutron signal and background requirements, (b) the requirements of experiments at ultra-low temperature and (c) the mechanical properties for work at high pressure. The techniques of the ^{3}He crystal growth at pressure between 4 and 6 MPa and at low temperature are described, together with a strategy for the crystal orientation and background reduction. As a result, large ^{3}He single crystals of good quality were obtained. With such samples, neutron experiments on magnetic order in solid ^{3}He at ultra-low temperature shift to the experimentally feasible regime.

(Some figures in this article are in colour only in the electronic version)

1. Introduction

The condensed ^{3}He isotope is a fermion system with spin $I = 1/2$ where, dependent on pressure and temperature, a complex diagram of liquid and solid phases is observed. A wealth of cooperative phenomena is found in the various phases. This comprises the superfluid states in the liquid phases as well as the observation of magnetic order both in the 2D and the bulk solid. The low mass of ^{3}He particles leads to large zero-point fluctuations. As one consequence, the liquid solidifies in the body-centred cubic (bcc) structure only under high pressure; a further increase of pressure then leads to the hexagonal close-packed (hcp) phase. The large delocalization of the ^{3}He particles with high probability causes an exchange of nuclei. These processes, which may involve two, three, and more particles, dominate the magnetic properties of the solid: they give rise to a direct exchange interaction which at temperatures below 1 mK leads to magnetic ordering [1]. Solid ^{3}He is the only system known with this direct exchange interaction and it is therefore a magnetic model system of central importance.

The phase diagram of the 3D solid shows three different magnetic phases: in the bcc phase at temperatures below 1 mK two of them are found, dependent on the applied external field (figure 1). In low field, a doubled unit cell with spin arrangement up–up–down–down (U2D2) is expected. In fields above 0.5 T, an antiferromagnetic structure without cell doubling, but with a canting of the moments into the field direction, is expected from the multiple particle exchange model [2]. This phase is usually called a 'canted nuclear antiferromagnet' (CNAF). Both structures can be distinguished uniquely using neutron diffraction: for the U2D2 and CNAF phases, characteristic $(\frac{1}{2}00)$ and (100) reflections are expected, respectively. Indeed, in one neutron diffraction experiment performed on solid ^{3}He in Grenoble [3], the U2D2 phase reflection has been observed once with a very low count rate. Unfortunately, the experiments there were not continued and this result was never reproduced. For completeness, we should

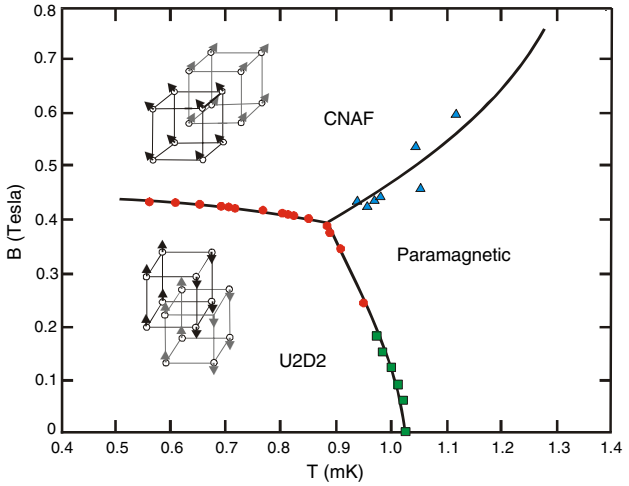

Figure 1. Phase diagram of solid ^{3}He in the low-pressure bcc phase. The magnetic structure figures show the proposed spin structures in the U2D2 and CNAF phases.

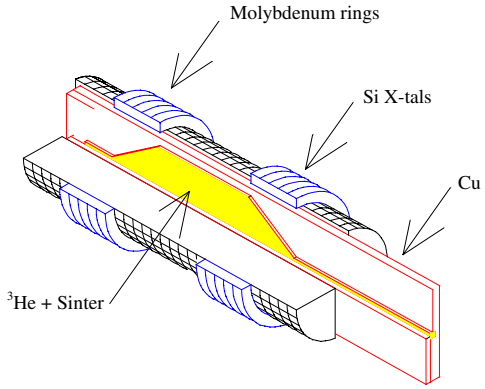

Figure 2. ^{3}He sample cell assembly. For details see the text.

mention that in the high-pressure hcp phase ferromagnetism has been observed at μK temperatures [4], in nice agreement with predictions of the multiple particle exchange model.

At the HMI in Berlin we have set up a new experiment to investigate the nuclear magnetic ordering of ^{3}He by means of neutron diffraction. Such experiments are difficult because high-pressure and ultra-low-temperature techniques must be combined with the neutron diffraction experiment. In addition, the very large absorption cross section of ^{3}He ($\sigma_{\mathrm{ABS}} = 5300$ barn) leads to a strong attenuation of the neutron signal, and the neutron capture decay products can heat up the sample with the excess energy of 760 keV. In the following we will describe the experimental methods to solve the conflicting requirements.

2. Sample cell

The sample cell consists of a Cu boat that contains the ^{3}He sample, clamped between two half cylinders cut from a Si single crystal to keep the forces under applied pressure. Mechanical stability is achieved by concentric rings of molybdenum pushed over the cylindrical assembly. Figure 2 shows a scheme of the sample cell assembly.

The ^{3}He sample is formed in a small volume between two Cu sheets. The shape of the sample volume is defined by an intermediate Cu layer of 100 μm thickness. The Cu cell is sealed by soft solder. In the beam area the volume is filled with sintered Ag powder (700 nm average particle size). On the one hand, the Ag sinter provides a large surface for cooling the sample below 1 mK. Equally important, the sinter provides an effective pathway to absorb the kinetic energy of the proton and tritium formed after neutron capture in ^{3}He: the corresponding absorption length in Ag is estimated to be around 1 μm, whereas the kinetic energy in ^{3}He will be absorbed only over distances as large as 30–60 μm. Thus only a small fraction of the neutron capture excess energy is deposited in the ^{3}He sample.

The Cu parts of the cell provide the thermal link to a powerful nuclear refrigerator. The covering Cu sheets are cut from high-purity foils of 200 μm thickness. The foils were heat-treated at 950 °C for 48 h, which resulted in a residual resistivity ratio RRR $\gg$ 1000. Using the Wiedemann–Frantz law, we estimate a thermal conductivity that is sufficient to keep the sample below 1 mk under a heat load of 20 nW expected from beam heating.

The reason for using very thin Cu foils for the sample cell is neutron background considerations. In the course of previous experiments it was realized that a cell made from 2 mm Cu sheets gave too high background due to incoherent scattering. Background considerations also dictated the choice of Si single crystals for the mechanical support structure. The perfect crystal structure of Si gives only a few, very sharp reflections but no diffuse background. Silicon is brittle, but otherwise it is an excellent choice because of its mechanical properties, e.g. the elastic modulus is superior to aluminium alloys, and the thermal contraction is small, i.e. the differential contraction tends to tighten the cell. The cell is kept together by two sets of concentric molybdenum rings. They have a conical shape, and the conical rings are pushed against each other with force to achieve a rigid cell.

The mechanical stability of the cell is important because 'small' deformations can be significant for a ^{3}He sample with an effective thickness of $\sim$60 μm. Cell deformations lead to volume elements that do not contain sinter. These parts of the sample would not cool; under the heat load of the neutron beam they heat up immediately and they reduce the neutron signal due to an unnecessary increase of absorption. Finally, with a mechanically unstable cell the control of sample growth is difficult because volume and pressure changes get coupled in an undefined way.

We have used neutron transmission experiments to determine the cell thickness and thus the deformation as a function of pressure. A wavelength of 1.4 Å was obtained from a Ge (220) monochromator. A sapphire crystal together with a pyrolitic graphite (PG) filter was used to remove the $\lambda/2$ contamination of the beam. Typically, the temperature of the cryostat was stabilized around 2.5 K, where the solidification occurs only at a pressure larger than 8 MPa; the corresponding maximum density is 140 kg m^{-3}. The pressure was increased

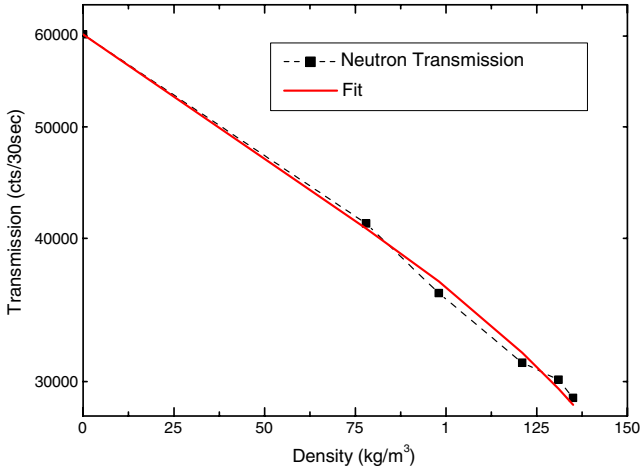

Figure 3. Neutron transmission as a function of ^{3}He density. Here the sample temperature was set to 2 K, and the density was adjusted with a change of the externally applied pressure between zero and 6.25 MPa. The straight line shows the transmission calculated with the fit. For details see the text.

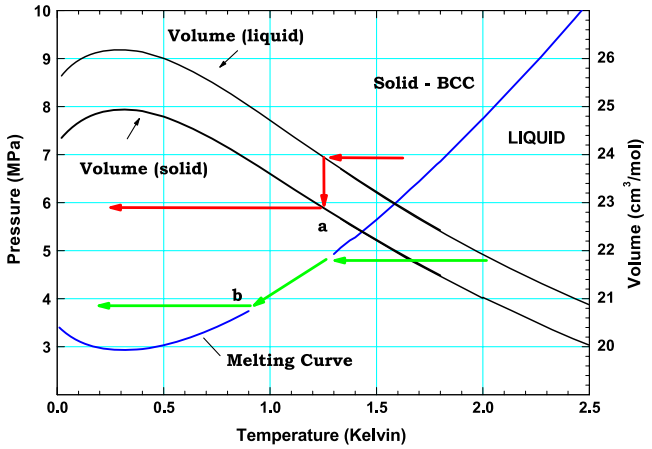

Figure 4. Liquid and solid density, melting curve.

in steps of 10 bar; after each change of pressure it took about 10 min to establish equilibrium in the sample cell. A pinhole of 2.3 mm diameter was set to probe the transmission in the centre of the sample.

The transmission data can be explained by assuming a linear change of the cell thickness as a function of pressure. We obtained the best fit for a cell deformation of $\Delta d = 0.015\ P[\mathrm{MPa}]d_0$ (figure 3). Thus, the maximum cell deformation was $\Delta d = 6\ \mu$m which compares reasonably to the initial ^{3}He thickness $d_0 = 60\ \mu$m. The deformation can also be calculated from simple mechanical formulae describing the bending of a slab under a distributed force. Using $\Delta d = 5\ Fl^3/384EJ$, where l is the length of the cell between the Mo rings (here $l = 20$ mm), E is the elastic modulus ($E_{\mathrm{Si}} \sim 120$ GPa), J the second moment of inertia and F the force, we arrive for our geometry at 3 μm deformation on either side of the cell. The result compares well with the measured data and shows that the Mo rings do not have appreciable deformation, in agreement with the expectation.

On the other hand, the results show that the parameter space for a stable cell is quite narrow: the cell deformation increases with the third power of the cell length and linearly with the force, that in turn is proportional to the cell length. Therefore, the cell deformation effectively increases with the fourth power of the cell length. It appears difficult to obtain a larger ^{3}He sample with an increase of the cell length without sacrificing the cell stability criteria. Increasing the width of cell could be a better possibility, but in our case this is limited by the diameter of the cryostat vacuum can.

3. Growth of ^{3}He single crystals

Above the minimum of the melting curve there are two principal methods of solidification: at constant pressure the solidification takes place at one temperature (point '**a**' in figure 4) and the volume changes by about 4% (figure 4, path 'A'). Conversely, at constant volume the pressure changes during solidification following the melting curve until point '**b**' is reached (figure 4, path 'B'). For this method additional ^{3}He must be supplied continuously to compensate the volume change. As the filling capillary usually blocks, this method requires special measures to heat the capillary. To avoid that complication, we usually prepared samples under constant volume conditions.

To keep the solid from melting at low temperatures, the final pressure should exceed 3.3 MPa; otherwise, the solid re-melts below the minimum of the melting curve. A second criterion for the final pressure is given by the strong dependence of the critical temperature for magnetic order on pressure and volume. To keep the ordering temperature as high as possible, the final pressure should be close to 3.3 MPa.

^{3}He samples were prepared at a starting pressure around 5 MPa, i.e. the solidification sets in at $T \sim 1.5$ K. As all dilution cryostats tend to show instabilities around 0.8 K, for sample growth pure ^{3}He was used to run the cryostat. The amount was adjusted so that no liquefaction occurred. With such settings, the temperature could be controlled well between 2 and 0.5 K, where all ^{3}He in the sample is solid. The cooling rate was chosen as slow as possible; the main limitation was the three-day time period between the regular refill of cryogenic liquids.

The growth was monitored by measurements of the sample density and pressure. The density in the centre of the sample cell was derived from the neutron transmission signal. A capacitive sensor at the mixing chamber was used to determine the pressure. The temperature of the sample cell and the mixing chamber was measured with two CERNOX sensors. Thermally, the sample cell and the pressure sensor are connected by high-conductivity metal. The difference between the two thermometers at the mixing chamber and the sample cell seen in figure 5 is within the calibration error. Nevertheless, a small temperature gradient leads to solidification of ^{3}He first inside the pressure cell. This leads to a reduction of the density in the sample cell due to the 4% density change upon solidification. Consequently, the liquid in the sample cell solidifies at a later stage. Another dead volume that leads to the same effect is the capillary connection between

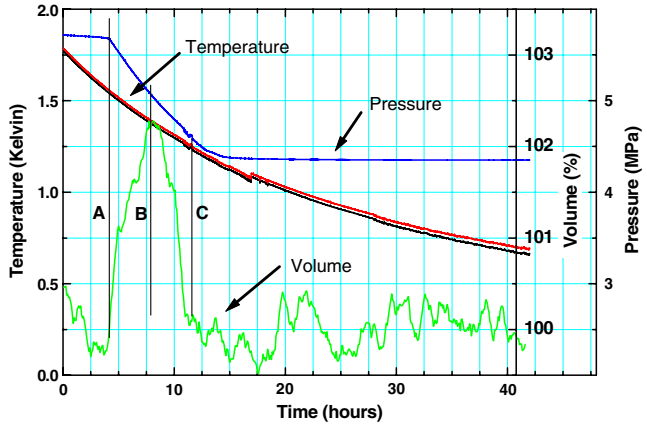

Figure 5. The figure shows a typical solidification process. The specific sample volume at 2 K was set to 100%. For details see the text.

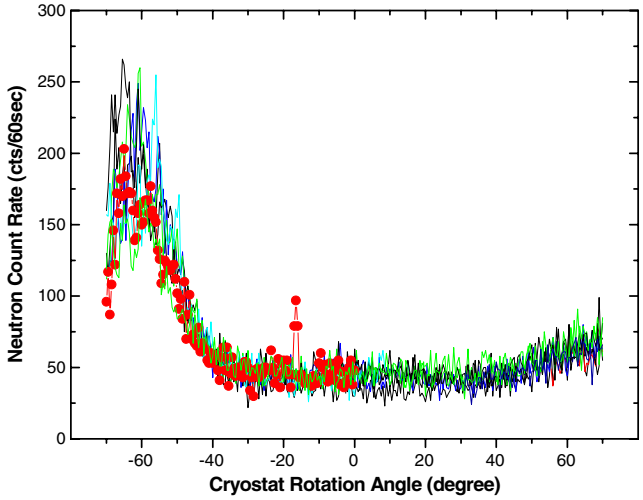

Figure 6. Results of several search scans with different detector inclination. The peak at −18° is a (110) reflection from ^{3}He. The scans shown in this figure differ in the detector inclination angle. For details see the text.

the pressure gauge and the sample. It has been carefully heatsunk over its entire length.

As an example, in figure 5 the solidification monitoring is shown. The starting pressure and temperature were determined in one or two 'fast' cool downs to start as close to the solidification point as possible in order to maximize the time for the solidification. A sharp kink of the pressure time dependence, marked by 'A' in figure 5, indicates the onset of solidification in the pressure gauge at $T = 1.5$ K, $P = 5.7$ MPa. The ^{3}He in the sample cell remains liquid, and due the liquid–solid density difference it moves from the sample cell to the pressure gauge. Consequently, the volume in the sample cell increases for a while. At 'B' the solidification starts in the sample cell, indicated by the maximum of volume in the cell. The solidification in the sample cell reverses the flow direction of the ^{3}He; this is likely connected with a partial remelting of solid ^{3}He in the pressure gauge. Only at 'C' is the specific volume in the sample cell constant, and is all ^{3}He in the pressure gauge and the capillary system solid.

The figure shows that neither of the ideal cases ('constant pressure' or 'constant volume' conditions) can be realized, despite the fact that the filling capillary is blocked above the mixing chamber. This is due to the significant amount of 'dead' volumes compared to the fairly small volume of the sample cell. Our attempts to model the pressure and volume dependence as a function of temperature have not been successful, likely due to the fact that the temperature gradients are not known with sufficient accuracy. We estimate the final pressure of the sample cell to be 4 MPa, somewhat above the ideal value of 3.3 MPa.

4. Orientation of ^{3}He single crystals

The bcc structure of solid ^{3}He shows reflections like (110), (200), (220), etc. In practice, due to the Debye–Waller factor, the reflections with higher indices are very weak. Therefore it is practical to orient the crystal using reflections of the (110) type. There are 12 reflections of this type; for orientation two, or in some cases three, independent (110)-type reflections are necessary. Because the orientation cannot be predicted from the crystal growth, the space must be scanned until one of these reflections is found.

Limitations come from the available range of diffractometer settings. For this reason the samples are oriented using a (220) Ge monochromator with a take-off angle of 42°. The resulting wavelength is 1.41 Å. The detector can be lifted by $+2°/-18°$. In principle, the cryostat can be rotated by ±90°. However, when the flat sample cell is rotated towards the parallel position with respect to the incident beam, the strong absorption hides reflections. Moreover, the parallel orientation opens a path for the incoming beam through the tight mask setting; consequently with large cryostat rotation angle the background increases. This causes the broad background peak seen in figure 6 at cryostat rotation angle −60°. Under such constraints, several samples could be oriented, which shows first that single crystals of ^{3}He can be obtained in the restricted geometry of a sinter and second, that these reflections can be seen with the diffractometer.

Figure 6 shows the result of typical search scans where the cryostat with the sample is rotated. The correct detector position with respect to the sample's lattice spacing is determined from the density of the sample. It is known from the growth conditions. The detector inclination is changed in steps of 2° to search for reflections above and below the diffractometer plane. Due to the above-mentioned absorption effect at large cryostat rotation angle, the first (110)-type reflection is usually found close to the centre of the search scan. The second reflection hides in the wings, and precise knowledge of the background structure is required to distinguish it from other signals.

On a different sample (figures 7(a) and (b)) we show the second step of sample orientation where two (110) reflections are obtained. The reflection in figure 7(a) is clearly weaker and suffers from higher background compared to the data in figure 7(b). This is due to the geometry effect mentioned above. Later, the scans were repeated with a liquid ^{3}He sample

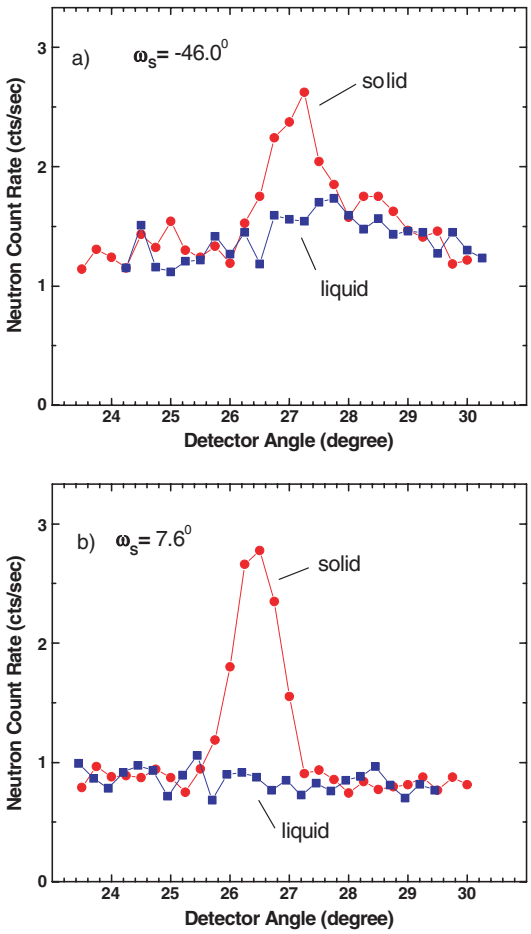

Figure 7. Two independent (110) reflections of solid ^{3}He. The counting time was 120 s per point. Here ω_S gives the cryostat rotation angle. For details see the text.

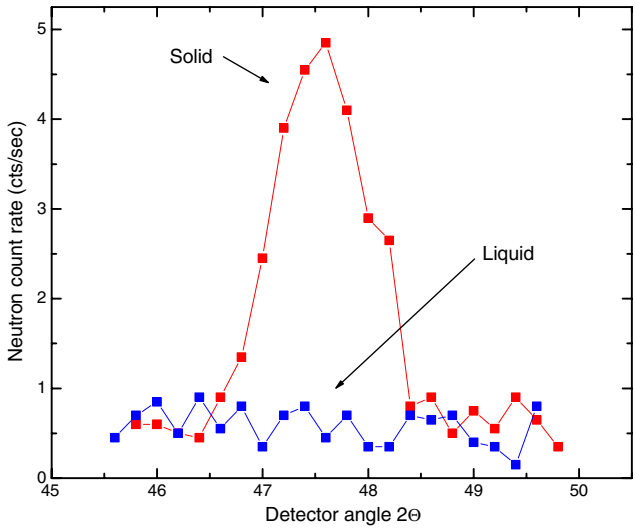

Figure 8. A ^{3}He-(110) reflection measured with a wavelength of 2.4 Å. Note the reduction of the background compared to similar data obtained at 1.4 Å.

of the same density to show that the signal is due to the solid ^{3}He.

With two independent reflections, the orientation of the sample is determined. It remains to discuss the signal size and the background. Using 1.4 Å wavelength the maximum signal on the (110) reflection was of the order of 2–3 cts s^{-1}. As regards the crystal preparation, there is little room for improvements: the sample scatters over its entire volume and the width of the reflections is close to the resolution limit. A small improvement of the single-crystal quality could be possible when the growth is further slowed down. Primarily this requires a reduction of dead volumes because the connected uncertainties have a direct effect on the control of the growth process.

The crystal growth in a sinter is not trivial: in earlier experiments it was realized that a single crystal grows only in low-density sinter (∼30% packing) and only over a length of 5 mm, starting from a triangular element above the neutron beam area that is free of sinter. Obviously, the sinter limits the coherent crystal growth and the resulting crystals do not fill the neutron beam area. On the other hand, ^{3}He easily forms crystals in an unrestricted volume. To improve the situation along the sinter the inner wall of the Cu sample cell was 'scratched' with a sharp needle over the entire cell length. Three such 'scratches' with an estimated cross section of approximately 10 μm^2 were applied on one side of sample cell. This provides small channels free of sinter where ^{3}He crystals can grow freely; they are thought to initiate crystal growth into the sinter with a short mean free path.

A second method of improving the signal/background ratio is a change of wavelength: among other parameters, a single-crystal reflection is proportional to $\lambda^3/\sin(2\Theta)$, where 2Θ is the scattering angle. The background is proportional to the flux. Thus, the use of longer wavelength can improve the signal/background ratio when the increased absorption is accounted for by a thinner cell. Another advantage is seen in the lower beam heating when the same signal/background ratio can be achieved with reduced neutron flux.

We have built a sample cell with thickness 60 μm because that optimizes the absorption at a wavelength of 2.4 Å. The sample had to be oriented at 1.4 Å; the higher wavelength does not give sufficient scanning range. After orientation, the wavelength was changed to 2.4 Å, obtained from a graphite monochromator. There we achieve a significant improvement of the signal/background ratio: it amounts to more than a factor of two (figure 8).

5. Summary

We have been able to prepare ^{3}He single crystals in a sinter suitable for investigations of nuclear spin order below 1 mK. The signal/background ratio in particular now has reached a value where the magnetic reflections from the nuclear ordering are in reach.

Acknowledgments

This project was started as a European Research Training network (RTN 2000166). We should like to thank the European Commission and the participants in that network for the continuous support in starting the experiments: E D Adams

(University of Florida, Gainesville, USA), J Goff (University of Liverpool, UK), J Saunders (University of London, UK), H Godfrin (CNRS Grenoble, France), M Roger (CEA Saclay, France) and E A Schuberth (Walther Meissner Institut, Garching, Germany).

References

[1] Osheroff D D 1992 *J. Low. Temp. Phys.* **65** 297
[2] Roger M *et al* 1983 *Rev. Mod. Phys.* **55** 1
[3] Benoit A *et al* 1987 *Can. J. Phys.* **65** 1343
[4] Lang T *et al* 1996 *Phys. Rev. Lett.* **77** 322